# Study of surface oxidation and recovery of clean $MoTe_2$ films

Trung, Pham Than; Castelino, Roshan; Felten, Alexandre; Sporken, Robert

*Published in:*
Surfaces and Interfaces

*DOI:*
10.1016/j.surfin.2021.101681

*Publication date:*
2022

*Document Version*
Peer reviewed version

Journal Pre-proof


# Study of surface oxidation and recovery of clean $MoTe_2$ films

Trung T. Pham, Roshan Castelino, Alexandre Felten, Robert Sporken

PII: S2468-0230(21)00752-5
DOI: https://doi.org/10.1016/j.surfin.2021.101681
Reference: SURFIN 101681

To appear in: *Surfaces and Interfaces*

Received date: 6 May 2021
Revised date: 7 December 2021
Accepted date: 12 December 2021

Please cite this article as: Trung T. Pham, Roshan Castelino, Alexandre Felten, Robert Sporken, Study of surface oxidation and recovery of clean $MoTe_2$ films, *Surfaces and Interfaces* (2021), doi: https://doi.org/10.1016/j.surfin.2021.101681

# Study of surface oxidation and recovery of clean $MoTe_2$ films

Trung T. Pham,[1,*] Roshan Castelino,[1] Alexandre Felten,[2] and Robert Sporken[1]

[1] *Namur Institute of Structured Matter (NISM), Department of Physics, University of Namur, 61 Rue de Bruxelles, B-5000 Namur, Belgium*

[2] *Technological Platform Synthesis, Irradiation and Analysis of Materials (SIAM), Department of Physics, University of Namur, 61 Rue de Bruxelles, B-5000 Namur, Belgium*

Transporting the sample through different characterization units while maintaining its integrity is crucial if multiple surface sensitive probes are to be employed. In this context, the layered transition metal dichalcogenides (TMDs) are known to be extremely susceptible to ambient degradation, leading to the formation of protrusions and particles on the films. Compared to $MoS_2$ and $MoSe_2$, $MoTe_2$ is one of the most reactive surfaces to ambient conditions. Therefore, understanding its surface oxidation and how to recover a clean surface is very important. In this paper, we report the MBE synthesis of single phase of $2\,H-MoTe_2$ with good stoichiometric films on graphene terminated $6H$-SiC(0001) substrates and are able to recover the clean surface after exposure to air under properly protected conditions. Our films are analyzed in detail by reflection high energy electron diffraction (RHEED), X-ray photoemission spectroscopy (XPS), and scanning tunneling microscopy (STM).



## I. INTRODUCTION

The layered quasi-two-dimensional transition metal dichalcogenides (TMDs) attract increasing research interest due to their particular electronic, optical, mechanical, chemical and thermal propertities [1–6]. Unlike graphene (a unique two-dimensional system), their electrical properties can vary from superconducting to metallic and to semiconducting with tunable bandgaps that undergo transition from an indirect one in bulk crystals to a direct one in monolayer films. Like other TMD materials, $MoTe_2$ exists in multiple phases among which the most stable phases are hexagonal ($2H$) and monoclinic ($1T'$). The $2H$ phase is semiconducting while the $1T'$ is semi-metallic. Monolayer $2H$-$MoTe_2$ has a direct bandgap about 1.1eV, the smallest among all semiconducting TMDs [7, 8], similar to the width of the indirect bandgap of Si. This makes it attractive for applications in electronics and optoelectronics. For the practical integration of $MoTe_2$ into devices, a thorough understanding of its surface and interfacial reactions is really needed.

A fundamental understanding of such reactions relies upon *in-situ* characterization methods conducted in ultra-high vacuum (UHV) in order to avoid contamination at the atomic level. In the present study, we have used molecular beam epitaxy (MBE) to grow high crystalline quality films with well controlled properties [9]. However, not all characterisation can be done in the same UHV unit and there is a need to move samples across characterization chambers.

A specific difficulty in surface science research and especially in the case of TMDs, is the transport of samples from one UHV system such as MBE to another system at a different location. TMDs are extremely susceptible to ambient degradation, displaying significant structural and morphological changes upon exposure to atmosphere [10]. Oxidation of the TMD thin films occurs preferentially at the grain edges inducing the formation of protrusions and

*Corresponding author: trung.phamthanh@unamur.be

particles on the films, leading to changes in the electronic properties of the films due to the formation of defect states [11, 12]. Besides the surface deformation, air exposure also results in an increase in the resistivity of the TMDs films and changes in the work function [13, 14]. This problem is more evident in the case of $MoTe_2$, one of the most reactive surfaces to ambient conditions as effects of the oxidation are visible after a few minutes of exposure to air [15, 16]. This oxidation is inevitable as TMD tellurides are more prone to oxidation than their sulphide or selenide counterparts [17, 18]. Therefore, transporting the sample through different characterization units while maintaining its integrity is crucial if multiple surface sensitive probes are to be employed.

A possible method for moving samples between UHV chambers without breaking vacuum is to use a vacuum suitcase [19]. The available commercial vacuum suitcases are equipped with an ion pump to maintain UHV conditions as well as several battery packs for independent power supply. However, the ion pump and the battery packs make the vacuum suitcase heavy and difficult to handle. Moreover, the use of vacuum suitcase often necessitates modifications of the configuration of the UHV system [20]. Alternatively, a widely used method is to protect the sample surface with an *in-situ* capping layer deposited at room temperature (RT) thick enough to prevent oxidation to reach the actual sample surface. This method is effective if the capping layer can be removed by heating in UHV after the sample has been transferred through air. In general, Te and Se have been used for capping MBE synthesized TMDs. The high vapour pressure of these species under moderate temperatures makes them good candidates for capping layers and these can be easily removed by moderate annealing while maintaining the integrity of the surfaces [21–23]. However, not all analysis chambers possess the facility for thermal anneal or can pump out relatively high vapour pressure materials like Se and Te that otherwise contaminate adjoining systems. In addition, if the annealing is not precisely monitored during decapping process, there is a risk that the deposited films will be damaged or even carried off along with the oxidized Te layers. Effects of such capping layers on $MoTe_2$ for preventing oxidation during transfer through air has not been reported yet.

**Through an understanding of the surface oxidation effect, one can stimulate the search for ways to preserve sample as long as possible for future applications. According to previous studies reported in literature, surface effects can significantly impact on the electrical transport properties [24–27]. Thus, it would be helpful for device fabrication if $MoTe_2$ TMD layers could present unaltered surface quality after exposure to ambient environment. Although it is highly desired, the studies of oxidation control have been rarely performed and characterized in details.** In this work, we make a systematic study of surface oxidation on $2H-MoTe_2$ as synthesized by MBE on graphene terminated $6H$-SiC(0001) substrates [9] and are able to recover the clean surface after passing through unavoidable air exposure for $ex-situ$ characterization. Under properly protected conditions, the sample can be reintroduced in the UHV chamber and a clean surface can be recovered with controlled annealing. Our films are analyzed in detail by reflection high energy electron diffraction (RHEED), X-ray photoemission spectroscopy (XPS), and scanning tunneling microscopy (STM).

## II. EXPERIMENTAL DETAILS

We use a kinetically controlled multi-step MBE process to synthesize large scale single-layer $2H$-$MoTe_2$ films on graphene as detailed in previous work [9]. Four sets of samples were produced with the same conditions (8-min deposition). Growth was monitored by reflection high energy electron diffraction (RHEED) (Riber). After growth,

samples were characterized by scanning tunneling microscopy (Park Autoprobe VP2 with an R9Plus controller from RHK Technology) and X-ray photoelectron spectroscopy (XPS) (K-Alpha spectrometer from Thermo Scientific with a monochromated Al K$\alpha$ X-ray source operating with an incident photon energy of 1486.6 eV). All measurements were made at room temperature. The scanning tunneling microscope is directly connected to the MBE chamber. Hence, STM images can be taken without exposing the samples to air. However, XPS is part of another UHV system, making transfer through air unavoidable. Before transfer of samples through air for XPS measurements, samples #2 and #4 are capped by a protective Te layer on top while samples #1 and #3 are not. Except for sample #1, other samples were placed in a clean dry box filled with nitrogen gas from a pressurized nitrogen gas cylinder ($\geq$99.9% pure) whenever they were removed from a UHV system.

Although several sets of samples were prepared, we present our results here based on one representative sample from each of the four sets which are labelled and organized in order as follows:

*Full exposure to air* ($\sim$ 24 hours): sample #1 ($MoTe_2$ surface without Te cap), and reloaded in UHV-STM for recovery after XPS.

*Preserved in nitrogen box* ($\sim$ 24 hours): sample #2 ($MoTe_2$ surface with Te cap, decapped in XPS chamber and transferred back into UHV - STM to check surface topography and re-annealed to clean its surface), sample #3 ($MoTe_2$ surface without Te cap, and reloaded in UHV - STM after XPS for annealing to clean its surface), sample #4 ($MoTe_2$ with Te cap, preserved in nitrogen box for the same 24 hours as sample #2 for comparison, then reloaded and decapped in UHV - STM).

## III. RESULTS AND DISCUSSION

Large STM image of pristine graphene and after formation of $2H$-$MoTe_2$ films on graphene of sample #1 are shown in Figs. 1(a) and 1(b), respectively. Single layer of $2H$-$MoTe_2$ can be observed together with a very small $2H$-layer on top. RHEED pattern in the inset shows the diffraction streaks from the $2H$-$MoTe_2$ deposited films and from the graphene substrate. The long streaks on RHEED pattern indicate a flat surface of the overgrown $2H$-$MoTe_2$ films. Indeed, the flat domains are visible in Fig. 1(b), covering almost the underlying graphene substrate.

Thanks to the different contrast between two materials, the small parts of the exposed graphene can still be observed; they are marked by 'G'. The atomic resolution image is easily obtained by zooming on a small area as indicated on Fig. 1(b). This kind of structure is typical of a $2\sqrt{3}$R30° Moiré pattern of monolayer $2H$-$MoTe_2$ on graphene which was already analyzed earlier [9] as shown in an inset of Fig. 1(b). It is evident that the as-grown layers are clean and of good crystalline quality. In order to investigate effects of air exposure on $2H$-$MoTe_2$ films, the sample was removed from the UHV chamber and exposed to air for nearly one day ($\sim$ 24 hours). Exposure to air leads to changes in surface quality as seen on a STM image of sample #1 in Fig. 1(c). Root-mean-square surface roughness increases from 0.33 nm before exposure to air to about 0.42 nm after exposure. RHEED also confirms the loss of crystallinity (see inset of Fig. 1(c)). The corresponding XPS survey spectrum of this sample #1 is shown in Fig. 2 (a). Besides the peaks from Te and Mo (from the $MoTe_2$ layer) and Si and C (from the substrate), there is a significant amount of oxygen contamination. The formation of Te-O and Mo-O bonds in the films is confirmed by the higher resolution spectra of Te 3$d$ (Fig. 2 (b)), and Mo 3$d$ (Fig. 2 (c)).

The oxide peaks are clearly visible on Te 3$d$ spectra (next to the Te-3$d_{\frac{5}{2}}$ and Te-3$d_{\frac{3}{2}}$ peaks) and Mo3$d$ spectra

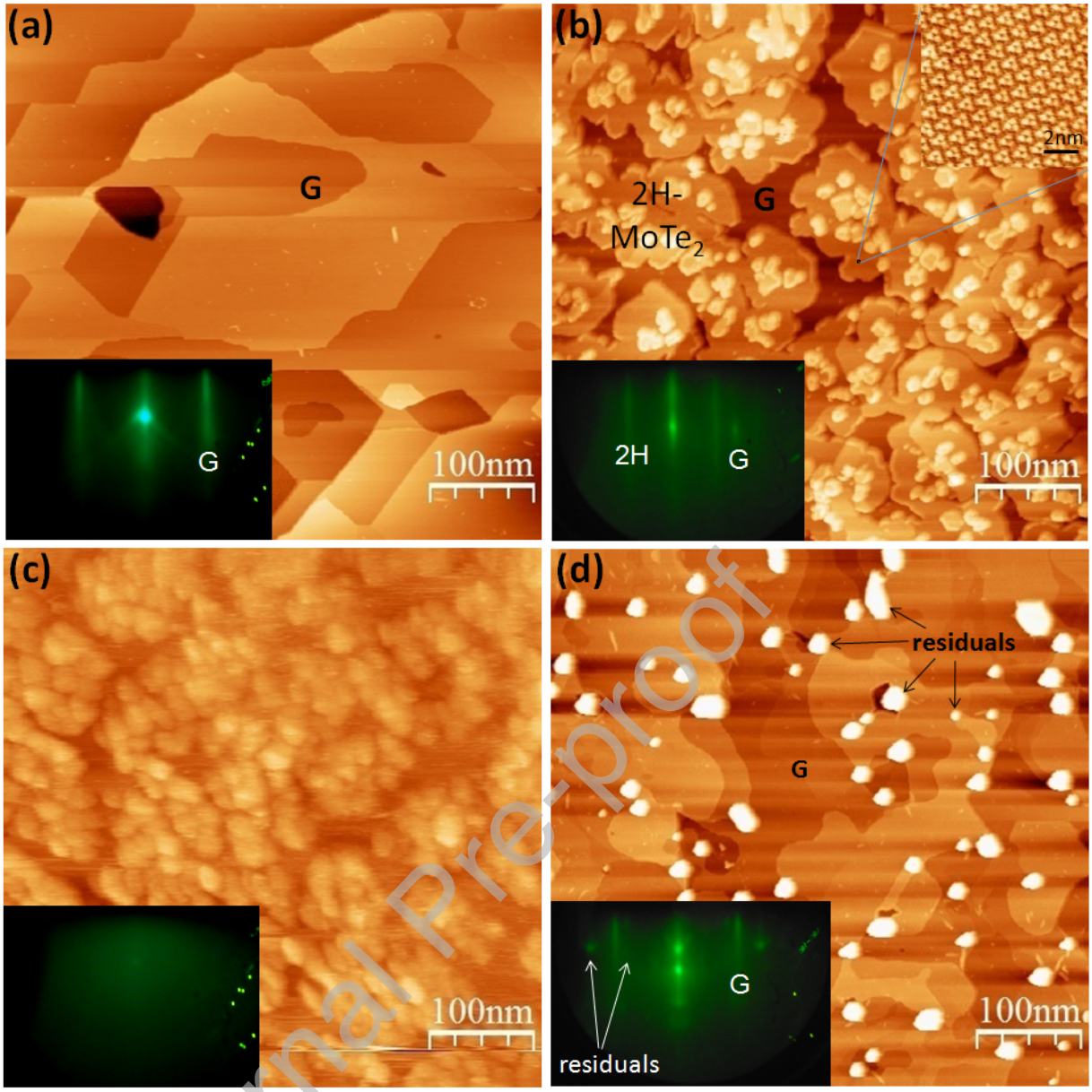


FIG. 1: 500×500 nm$^2$ STM images of sample #1: (a) Pristine graphene on terminated 6$H$-SiC(0001) substrates ($V_{Sample}$ = +1 V, $I_{Tunnel}$ = 1000 pA) with the corresponding RHEED pattern from graphene. (b) after $MoTe_2$ growth with parts of the underlying graphene substrate as indicated by G ($V_{Sample}$ = −0.5 V, $I_{Tunnel}$ = 600 pA). The inset shows the RHEED image confirming the epitaxial growth of $MoTe_2$ on graphene together with an atomic resolution image in the inset showing a typical Moiré pattern of the $2\sqrt{3}$R30° monolayer 2$H$-$MoTe_2$ on graphene ($V_{Sample}$ = +0.2 V, $I_{Tunnel}$ = 1300 pA). (c) Surface topography of the $MoTe_2$ films after full exposure to air ($V_{Sample}$ = +1.3 V, $I_{Tunnel}$ = 500 pA) together with the RHEED pattern in the inset. (d) after annealing the sample in UHV - STM at ∼ 350°C ($V_{Sample}$ = −0.5 V, $I_{Tunnel}$ = 200 pA).



(denoted as $MoO_2$ and $MoO_3$ by peak fittings), confirming oxidation of both Mo and Te in the $MoTe_2$ films.

The question is how to remove this oxide layer and recover the clean $MoTe_2$ films in a UHV chamber. Starting with sample #1, we gradually increased the sample temperature to 200°C while monitoring with RHEED, but the diffraction streaks of $MoTe_2$ did not appear (see Supporting Information Fig. S1). Thus, annealing was further continued up to 350°C. The substrate is maintained at this temperature for few minutes and RHEED pattern apprears

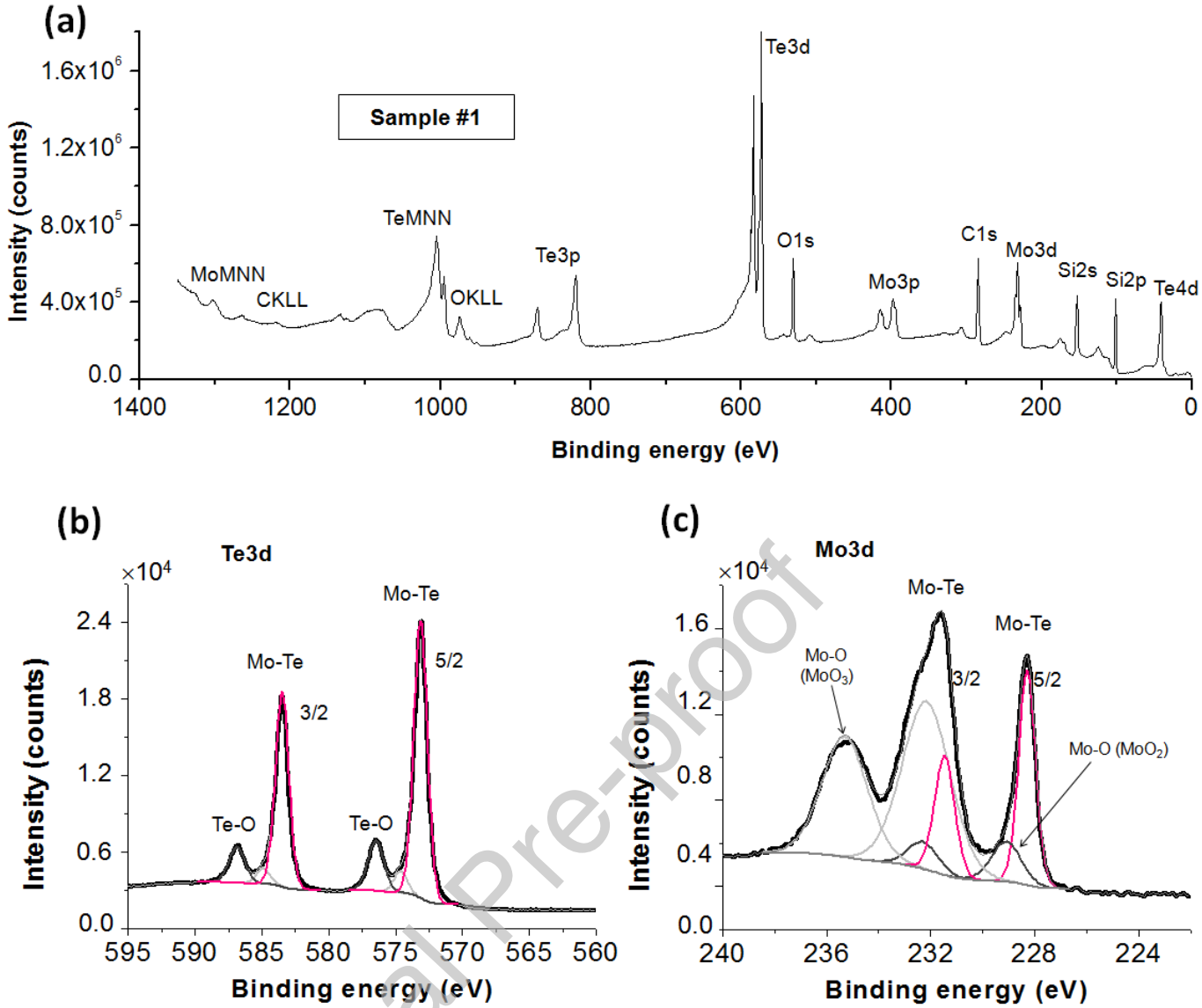


FIG. 2: XPS analyses of corresponding sample #1 after full exposure to air for handling XPS spectroscopy: (a) General survey showing quite high O 1*s* peak, indicating heavy surface oxidation. (b) a zoom-in of Te 3*d*, and (c) Mo 3*d*.



and then, allowed to cool it down to RT. **STM topography image shows large areas of graphene and some remaining bright spots on the surface (Fig. 1 (d)) which could be from residual Mo bonded on the substrate (marked by black arrows). These contaminants are also visible in RHEED (see the inset) which shows some spots and very faint streaks near graphene.** It is clear that graphene is recovered, but $MoTe_2$ is also removed by such heat treatment.

Actually, it is expected to see graphene instead of $MoTe_2$. Indeed, as $MoTe_2$ binds to graphene mainly through Van der Waals interaction, heating to a temperature that is sufficient to decompose $MoO_3$, $MoO_2$ and $TeO_2$ oxides will also lead to desorption of $MoTe_2$. Such behaviour has been observed on several samples, despite very accurate control of the sample temperature.

In order to protect the $MoTe_2$ films, a layer of pure Te was deposited before removing the samples from the UHV

system. The capping layer must be thick enough to prevent oxidation of the underlying $MoTe_2$. However, they should not be unnecessarily thick because this would make their subsequent removal more difficult. Without a real-time monitoring technique like RHEED, there is a risk of damaging the $MoTe_2$ surface unless a precise calibration of removal process for each of the UHV chambers is done beforehand. **A few samples of $MoTe_2$ with such a coverage of the thin Te capping layer were produced and followed by the same air exposure as sample #1, then the annealing was also performed in the same UHV chamber, but the crystalline quality of the films could not be recovered (not shown here).** From this fact, one can conclude that a full exposure of $MoTe_2$ films with or without a coverage of protective Te layers to air always induces a heavy oxidation of the sample and degrades the crystalline quality of deposited $MoTe_2$ during annealing to recover the clean films.

To prevent surface oxidation due to air exposure during transportation as much as possible, we use a dry nitrogen box for the transfer process. From the MBE chamber, the samples with or without a protective layer can be transferred to the box. Details of transfer process are shown in supplementary information (Fig. S2). We compare the XPS spectra of two samples: sample #2 ($MoTe_2$ capped with Te and decapped in XPS chamber) and sample #3 ($MoTe_2$ preserved in nitrogen box without Te cap) to understand the surface behaviour.

In order to compare the Mo-Te peaks before and after decapping Te layers, we work with thin capping layers; otherwise only Te peak from protective Te layers would be detected. Another advantage of thin capping layers is that they need only short annealing at moderate temperatures for their removal. **In this work, the thickness of protective Te layer is estimated about 5nm.** The XPS spectra of sample #2 (capped with Te in MBE chamber and subsequently uncapped in the XPS at $\sim 200°C$ for 10min under a base pressure $\sim 10^{-8}$ mbar) together with sample #3 without protective Te layer are shown in Fig. 3.

With a protective Te layer on the $MoTe_2$ surface, the XPS survey spectrum shows a very small Mo 3d peak located at $\sim 228$ eV which could be still visible while the Te 3$d$ peak at $\sim 573$eV is broad and quite strong (Fig. 3(a)). This signal is dominated by the Te capping layers rather than from the underlying $MoTe_2$ layers due to the thick protective Te films formed on top. Details in the formation of Te-Te and Mo-Te bonds will be examined later by focussing on the higher resolution spectra of Te 3$d$ and Mo 3$d$ in Fig. 4. When the sample is heated to desorb Te atoms, the surface composition is recovered (Fig. 3(b)). Comparison of spectra from $MoTe_2$ transferred under nitrogen atmosphere (Fig. 3(c)) and samples coated with Te and decapped after transfer through nitrogen atmosphere (Fig. 3(b)) show that both methods produce samples with similar surface composition. However, there is the small oxygen contamination after decapping which comes from outgassing during heating sample #2 in the XPS chamber, as this system is not optimized for heating under UHV conditions.

More information about surface chemistry is obtained from Mo 3$d$ and Te 3$d$ spectra as shown in Fig. 4 in combination with a summary of the stoichiometric determination from XPS spectra as given in Table I. We analyze spectra from sample #2 ($MoTe_2$ coated with Te and transferred through nitrogen box) before and after heating in the XPS system and those from sample #3 ($MoTe_2$ transferred through nitrogen box). For $MoTe_2$ coated with Te, Fig. 4(a) shows the Mo-3$d_{\frac{3}{2}}$ and Mo-3$d_{\frac{5}{2}}$ peaks corresponding to Mo-Te bonds at $\sim 231.34$ eV and $\sim 228.15$ eV respectively. These peaks are strongly attenuated by the Te capping layer. However, the peaks are enhanced after recovering the sample surface due to increased detection of the Mo-Te bonds in the $MoTe_2$ films (Fig. 4(b)) and are located at $\sim$ 231.43 eV and $\sim 228.24$ eV respectively. These values are very close to those of sample #3, where Mo-3$d_{\frac{3}{2}}$ and Mo-3$d_{\frac{5}{2}}$ peaks corresponding to Mo-Te bonds occur at $\sim 231.43$ eV and $\sim 228.28$ eV respectively (Fig. 4(c)).

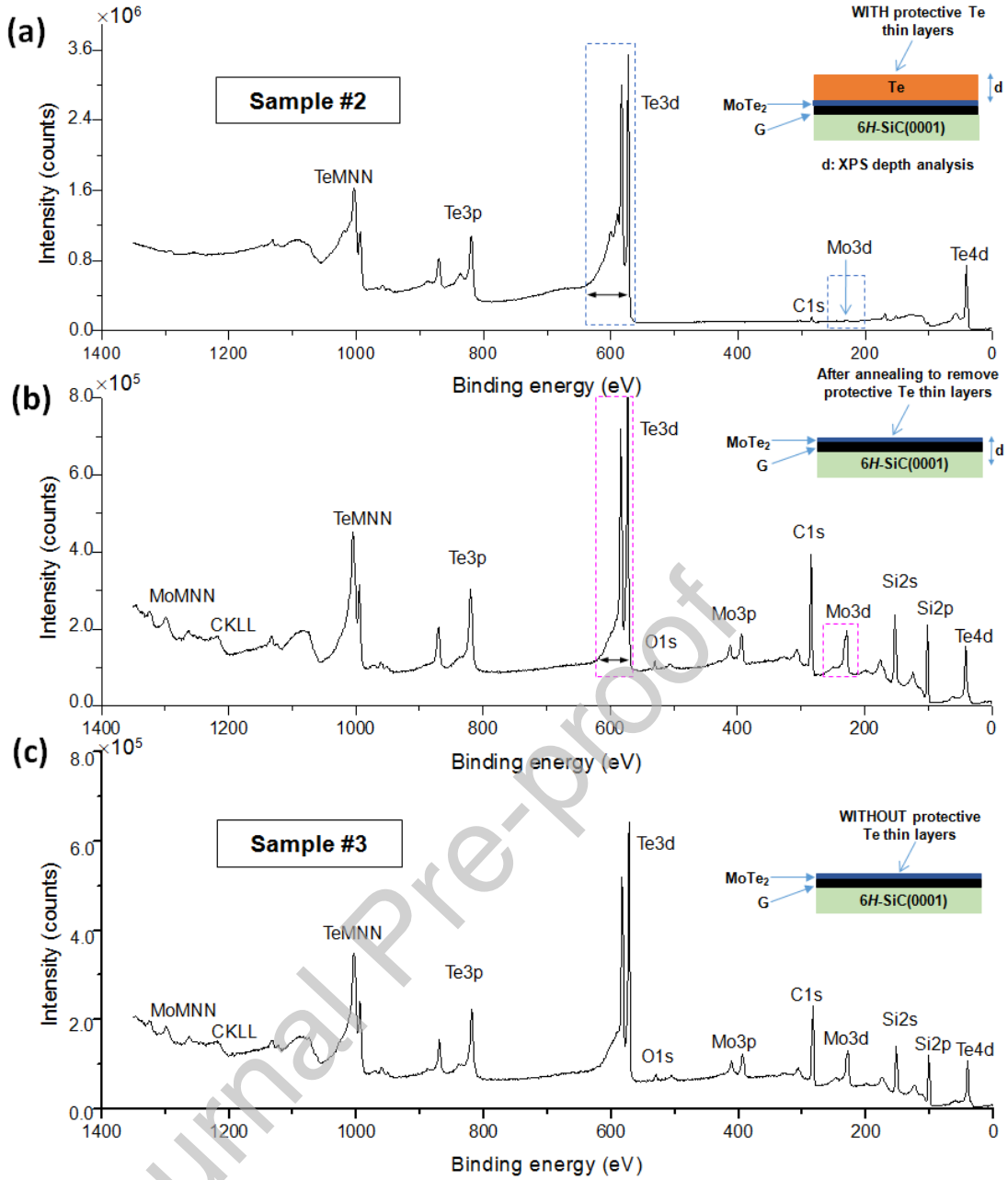


FIG. 3: Survey XPS spectra of samples #2 and #3: (a) Sample #2 capped with Te in UHV-STM, (b) After the removal of the capping layer in XPS chamber. The difference on the vertical intensity scale is highlighted. XPS depth analysis is indicated by d. (c) Sample #3 without protective Te layer for comparison with sample #2 after decapping.

Te-3$d_{\frac{3}{2}}$ and Te-3$d_{\frac{5}{2}}$ peaks corresponding to Mo-Te and Te-Te bonds for the capped sample are located at $\sim$ 583.43 eV and $\sim$ 573.04 eV respectively (Fig. 4(d)). The Te cap contributes strongly to the Te signal. A plasmon loss (marked by Te$^*$ in the red box) at $\sim$ 591 eV is attributed to elemental Te. Once annealed, the plasmon satellite peak disappears (Fig. 4(e)). The Te-3$d_{\frac{3}{2}}$ and Te-3$d_{\frac{5}{2}}$ peaks corresponding to only Mo-Te bonds occur at $\sim$ 583.45 eV and $\sim$ 573.06 eV respectively. After heating, the full width at half maximum (FWHM) of Te-3$d$ peaks increases from 0.85 eV to 0.93 eV. This is due to the fact that the Te signal comes from Te in $MoTe_2$ rather than elemental Te. For sample #3, the Te-3$d_{\frac{3}{2}}$ and Te-3$d_{\frac{5}{2}}$ peaks corresponding to Mo-Te bonds are located at $\sim$ 583.47 eV and $\sim$ 573.07

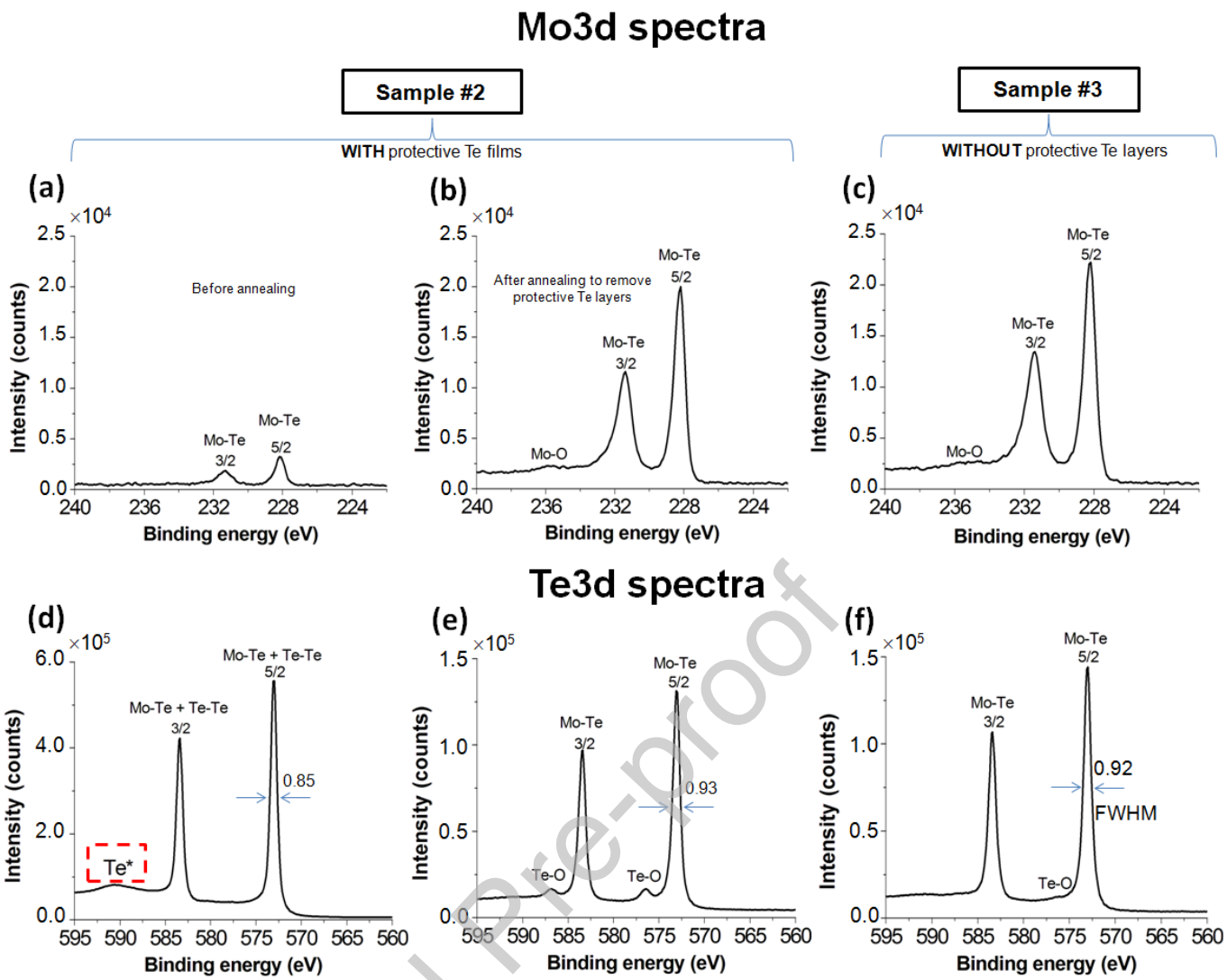


FIG. 4: Mo 3d and Te 3d spectra of samples #2 and #3: (a) and (b) Mo 3d spectra of sample #2 capped with Te and uncapped in XPS respectively. (c) Mo 3d spectra of sample #3 without protective Te layer. Corresponding (d) and (e) Te 3d spectra of sample #2 capped with Te and uncapped in XPS respectively. The boxed region in (d) corresponds to the plasmon loss due to metallic bonding of elemental Te. (f) Te3d spectrum of sample #3.

eV respectively (Fig. 4(f)). Their FWHM is $\sim$ 0.92 eV, very similar with the one of sample #2 after removing the protective Te layer.

After thermally removing the Te cap layer, small oxide peaks appear at 236 eV (Mo-3$d$, Fig. 4(b)) and near 576 eV and 587 eV (Te-3$d$, Fig. 4(e)). They are due to the presence of $MoO_3$ and $TeO_2$ [28, 29]. As mentioned earlier, such surface oxidation is related to the annealing of the sample in the XPS chamber where the sample holder is not designed for heating samples under UHV conditions. Compared to sample #3, the intensity of Mo-Te peaks of sample #2 after annealing are very similar, confirming the successful removal of protective Te layers. In addition, sample #2 is re-annealed in the UHV-STM chamber (under a base pressure $\sim 10^{-11}$ mbar) to improve its surface quality and another XPS measurement was taken (see the numerical results in Table I).

**One can see the relative upshift in Mo-Te peaks of Mo 3$d$ and Te 3$d$ of sample #1 with a full coverage**

| Sample No. | Sample status | Sample surface | Binding energy (eV)* | | | | ΔE(eV) Mo-Te $3d_{5/2}$ | Atomic ratio (Te/Mo) | Ref. |
|---|---|---|---|---|---|---|---|---|---|
| | | | Mo3d | | Te3d | | | | |
| // | // | // | $3d_{3/2}$ | $3d_{5/2}$ | $3d_{3/2}$ | $3d_{5/2}$ | // | // | // |
| #1 | full exposure to air | without protective Te layers | 231.46 | 228.32 | 583.51 | 573.13 | 344.81 | 2.18 | This work |
| #2 | preserved in dry $N_2$ box | with protective Te layers | 231.34 | 228.15 | 583.43 | 573.04 | 344.89 | 77.62 | This work |
| | | after annealing in XPS to recover $MoTe_2$ | 231.43 | 228.21 | 583.45 | 573.07 | 344.86 | 2.44 | This work |
| | | after re-annealing in UHV | 231.40 | 228.30 | 583.47 | 573.07 | 344.77 | 1.98 | This work |
| #3 | preserved in dry $N_2$ box | without protective Te layers | 231.43 | 228.28 | 583.47 | 573.07 | 344.79 | 2.15 | This work |
| Reference sample | CVD synthesis | single crystal | 231 | 227.8 | 583 | 572.6 | 344.80 | 2.125 | [29] |

*Graphene: C1s ∼284.6 eV.

TABLE I: XPS analyses of various samples

**of oxide layers compared to samples #2 and #3 (preserved in dry $N_2$ box). This can be explained by the higher electronegativity of oxygen compared with Mo and Te atoms which results in a decrease of the electron density around Mo and Te leading to the increase in binding energy [6, 15]. The up-shifting to higher binding energy of Mo-Te peaks after oxidation of $MoTe_2$ films by air-exposure is also reported by Diaz et al. [30]. The upshift in these cases is not due to the doping effects. However, it is worth noting that Refs. [16, 31] reported the downshift of the Mo-Te peaks in Mo 3$d$ and Te 3$d$ to lower binding energy after surface oxidation via $O_3$ exposure [16] or by $O_2$ plasma treatments [31] which are attributed to hole doping effects in $MoTe_2$ films. The possible explanation for the discrepancy between our results and literature in this aspect is derived from the different mechanisms of oxygen exposure. In our case, the $MoTe_2$ surface is gradually oxidized under the exposure of sample to air (sample #1 with full exposure) with the fact that MBE-grown $MoTe_2$ has the superclean surface with the chemical instability due to the weak Mo-Te bond energy as reflected in the small electronegativity difference between Mo and Te [32]. As a result, amorphous oxide layer is completely covered on the surface. The broadening and shifting in the Mo-$3d_{\frac{3}{2}}$ peak (see Fig. 2 (c)) toward higher binding energy suggests that oxidation strongly occurred in the sample rather than doping effects. For less oxidized samples #2 & #3, the oxidation effect is very weak, the position of Mo-Te peaks is almost not shifted as expected.**

By measuring the integrated peak area (I) and using sensitivity factors (SF) 5.4, 1.66 corresponding to the peaks Te-$3d_{\frac{5}{2}}$, Mo-$3d_{\frac{5}{2}}$ respectively, the atomic ratio can be calculated by [33]

$$\frac{\mathrm{Te}}{\mathrm{Mo}} = \frac{\mathrm{I}_{\mathrm{Te}3d_{\frac{5}{2}}}/\mathrm{SF}_{\mathrm{Te}3d_{\frac{5}{2}}}}{\mathrm{I}_{\mathrm{Mo}3d_{\frac{5}{2}}}/\mathrm{SF}_{\mathrm{Mo}3d_{\frac{5}{2}}}}$$

Comparing the Te:Mo ratio with the single crystal of 2$H$-$MoTe_2$ as reported by Bernede et al. [29], it can be concluded that sample #2 (after annealing in UHV) and sample #3 present stoichiometric films.

Further characterization was focussed on the O 1$s$ spectrum of all measured samples for comparison in Fig. 5. For better evaluation, the surface topography of corresponding samples is also shown together in the inset. With the same vertical scale for all the spectra, it is obvious that the amount of oxygen varies strongly among different samples. The highest intensity of the O 1$s$ peak is observed on sample #1 (full exposure to air) in Fig. 5 (a) while there is little oxide on sample #3 (preserved in the dry $N_2$ box) in Fig. 5 (d). Some oxide appears in sample #2 after removing the Te cap layer in XPS chamber (see explanation above) in Fig. 5 (c). Compared to samples #1 and #2 (after decapping), the surface of sample #3 exhibits the lowest surface oxidation.

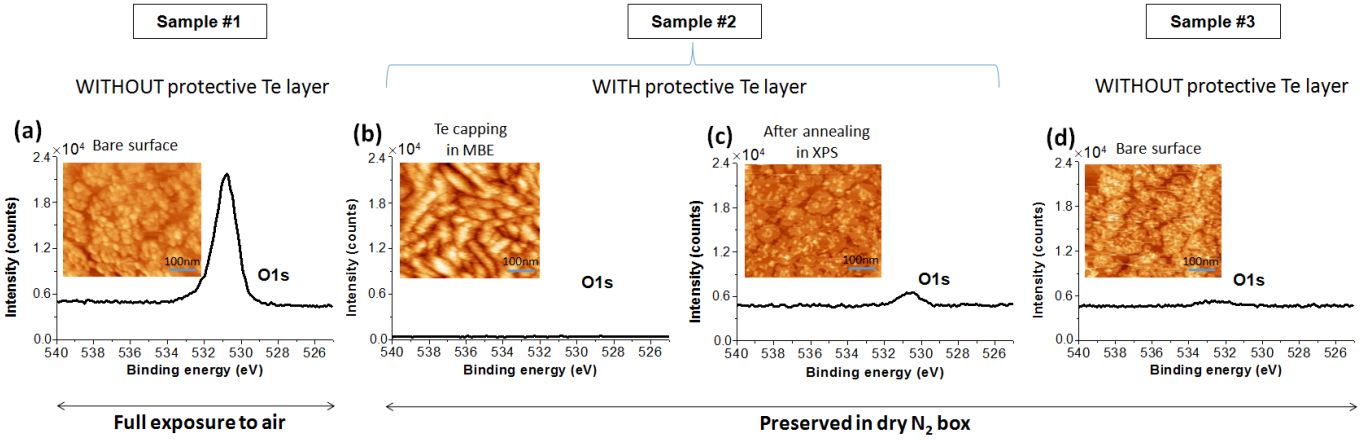


FIG. 5: The O 1*s* core level on corresponding samples showing different topographic images as seen in the inset, respectively: (a) #1, (b) #2 (with capped Te layer in MBE chamber) and (c) with decapped Te layer in XPS chamber, (d) #3 for comparison between different degrees of surface oxidation.

To confirm the surface structure, STM images are acquired for samples #2 and #3 as shown in Fig. 6. First, large scale STM images were taken on sample #2. The as-grown sample (Fig. 6(a)) reveals a uniformly distributed $2H$-$MoTe_2$ domains on graphene.

The single-crystalline quality of $2H$-$MoTe_2$ films is confirmed by bright RHEED diffraction streaks in the inset. After the deposition of the capping Te layer on the surface (Fig. 6(b)), the surface becomes quite rough, as expected for room temperature deposition, with a root mean square (RMS) roughness $\sim 0.5$ nm compared to $\sim 0.28$ nm for bare $2H$-$MoTe_2$ films/graphene on this sample. The RHEED pattern in the inset shows only diffraction streaks from such a rough Te capping layer. $2H$-$MoTe_2$ streaks are no longer observed, indicating that the surface is completely covered by Te. The sample is decapped in the XPS chamber as seen in Fig. 6(c). Although the surface topography shows a recovery, STM image indicates an unclean surface with non-ideal scanning conditions which could be due to the residual oxide formation as suggested by the XPS characterization (see Figs. 4(b) & (e)). Indeed, the corresponding RHEED pattern in the inset shows very faint streaks, suggesting that the surface is still contaminated. Annealing the film in UHV-STM chamber later cleans the sample surface as confirmed by STM image with its corresponding RHEED pattern in the inset of Fig. 6(d).

The as-grown sample #3 also shows flat domains of $2H$-$MoTe_2$ with a nice RHEED pattern in the inset (Fig. 6(e)), similar to sample #2. After XPS measurement (the XPS analysis was performed on this sample without the annealing treatment), the sample is reloaded in the UHV - STM chamber and its surface is checked. Although STM image is not really sharp, the surface of sample #3 still shows domains of $MoTe_2$ (Fig. 6(f)), indicating that its surface is much less contaminated than that of sample #1 after full exposure to air (Fig. 1(c)). Then, the sample was annealed at $\sim$ 200°C for 10min and the result is shown in Fig. 6(g). The crystalline quality of recovered films can be confirmed by corresponding RHEED pattern in the inset and its STM image in Fig. 6(h).

For practical applications, it may be necessary to store samples outside of UHV conditions for extended periods. In order to check the effect of such extended storage, we have removed sample #3 from the UHV chamber, kept it in the dry $N_2$ box for one week and then, reloaded into the UHV system. STM shows that the crystalline quality of $MoTe_2$ is preserved (supplementary information Fig. S3).

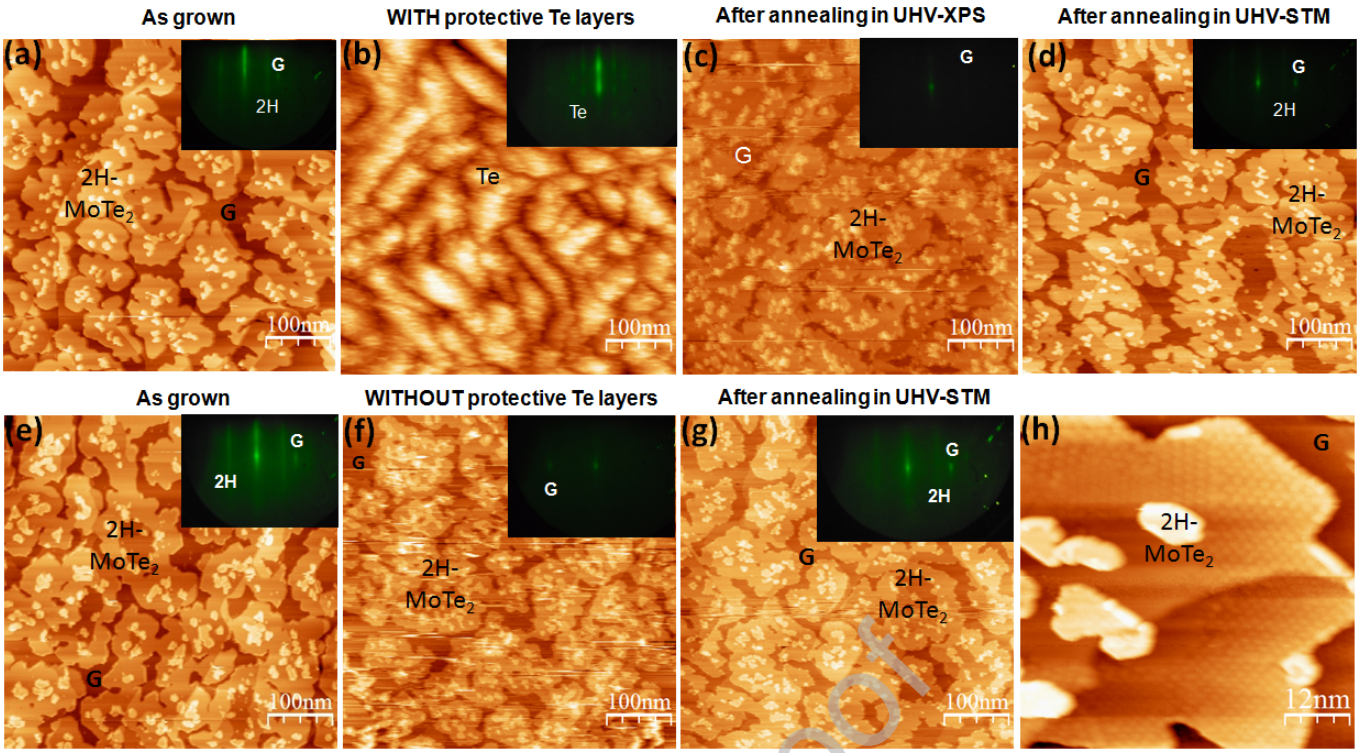


FIG. 6: STM images of sample #2: (a) As-grown surface ($V_{Sample} = -0.5$ V, $I_{Tunnel} = 700$ pA), (b) STM image after the deposition of Te capping layer ($V_{Sample} = +2.5$ V, $I_{Tunnel} = 1000$ pA), (c) The sample after desorbing the Te layer in XPS chamber ($V_{Sample} = -1.6$ V, $I_{Tunnel} = 1000$ pA), (d) Recovered sample after re-annealing in the UHV-STM ($V_{Sample} = -0.6$ V, $I_{Tunnel} = 1400$ pA); STM images of sample #3: (e) As-grown surface ($V_{Sample} = -0.5$ V, $I_{Tunnel} = 1000$ pA), (f) The surface topography after XPS measurment ($V_{Sample} = 0.7$ V, $I_{Tunnel} = 1300$ pA), (g) The recovered surface after annealing in UHV-STM ($V_{Sample} = +1.4$ V, $I_{Tunnel} = 400$ pA), (h) Close-up STM image confirms the clean $MoTe_2$ surface ($V_{Sample} = -0.8$ V, $I_{Tunnel} = 400$ pA). RHEED patterns are attached in the inset of corresponding STM images for crystalline quality reference.

To further understand the effect of annealing in UHV to recover a clean $MoTe_2$ surface, we prepared another sample capped with a Te layer and kept in a dry $N_2$ box for 24 hours and then, re-introduced in the UHV-STM chamber to remove the protective Te layers. This is very similar to sample #2; the only difference is that the Te layer was desorbed in the STM system instead of the XPS chamber and that XPS spectra were not recorded on this sample. This sample is labelled as sample #4 and shown in Fig. 7.

The surface topography of sample #4 displays clean domains of $MoTe_2$ on graphene, very similar to sample #2 (Fig. 7(a)). A height profile along the blue line shows the height of monolayer between 5 Å to 7 Å. This height is consistent with the model outlined in previous work [9]. The root mean square (RMS) surface roughness is $\sim 0.3$ nm. Next, a capping layer of Te is deposited on this sample (Fig. 7(b)). Irregularly formed islands cover the surface, inducing higher surface roughness ($\sim 0.5$ nm). Only RHEED diffraction streaks from such Te capping layers are observed, $2H$-$MoTe_2$ streaks are no more detected as seen in the corresponding inset. After keeping the sample in a dry $N_2$ box for 24 hours, it is reintroduced in the UHV-STM chamber and slowly annealed up to 200°C (10min). RHEED pattern in the inset of Fig. 7(c) after removing the protective Te layers is quite bright with clear diffraction streaks for $MoTe_2$, nearly the same as the pristine pattern in Fig. 7(a). The topography image is also very similar to the pristine surface with almost the same height of the monolayer as indicated in the height profile along the red line

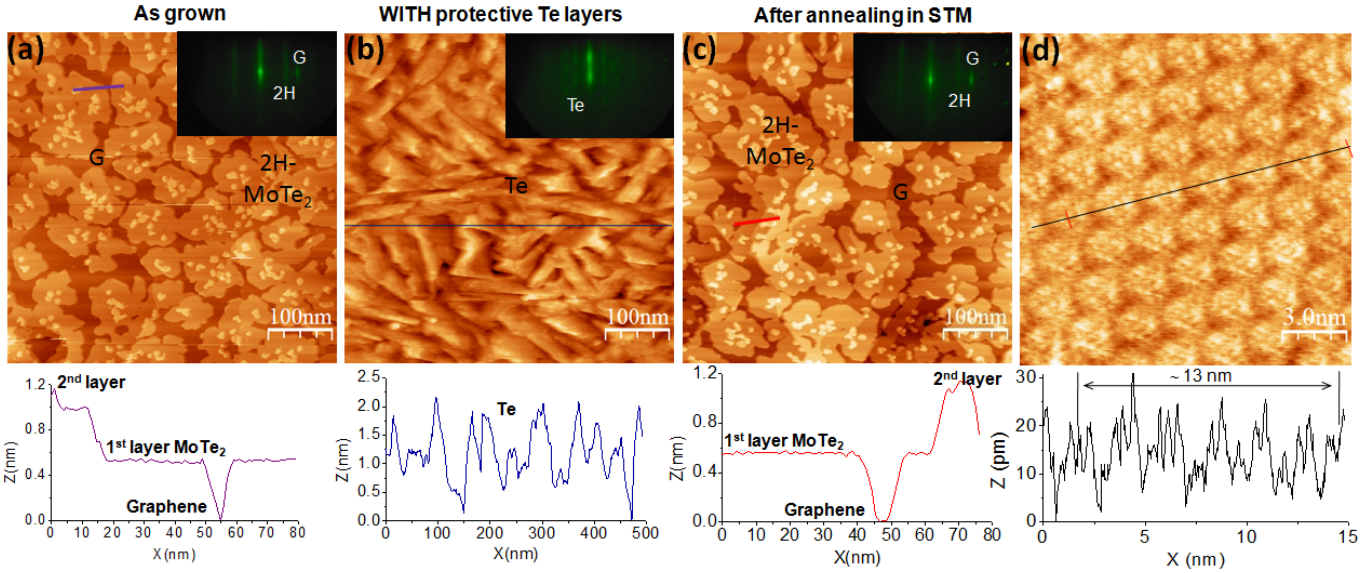


FIG. 7: STM images of sample #4: (a) As-grown surface of $2H$-$MoTe_2$ ($V_{Sample} = -0.5$ V, $I_{Tunnel} = 700$ pA), (b) STM image after the deposition of Te capping layer ($V_{Sample} = -0.5$ V, $I_{Tunnel} = 1000$ pA), (c) recovered sample after reloading and annealing in UHV-STM ($V_{Sample} = -0.5$ V, $I_{Tunnel} = 600$ pA), and (d) Atomic resolution was nicely observed after recovering $2H$-$MoTe_2$ ($V_{Sample} = -0.2$ V, $I_{Tunnel} = 2000$ pA). RHEED patterns are attached in the inset of corresponding STM images. In each image, the height profile along the line is given below, respectively. G stands for graphene and $2H$ stands for $2H$-$MoTe_2$.

and a nice atomic resolution from the $\sqrt{39}$R33.2° Moiré pattern of monolayer $2H$-$MoTe_2$ on graphene was obtained (Fig. 7(d)), confirming perfect recovery of sample #4.

From XPS analysis, one can see that a reasonably pure Mo-Te peak is present in sample #3 (see supporting information in Fig. S4). Although its STM image shows instabilities, domains of monolayer $2H$-$MoTe_2$ can still be observed. Unlike sample #1 (full exposure to air), the surface of sample #3 (preserved in $N_2$ box) still remains quite good quality after transportation through air. Between samples #2 and #4 (capped with protective Te layers), sample #4 shows much better surface quality after decapping in UHV-STM, comparable to its pristine surface. Compared to sample#3 (without capped Te layers), the surface of sample #4 has slightly better quality after annealing to desorb the oxide layers as can be seen on its stable STM image. This can be understood by the direct exposure of the $MoTe_2$ surface to air during transferring process (even very short time) of sample #3 which also makes it difficult to remove any remaining oxide due to strong covalent Te-O and Mo-O bonds in the films. **From experiments, one can suggest that capping the sample with protective Te layers and storing in a dry $N_2$ box (sample #4) would perfectly protect the $MoTe_2$ films from any contact with oxygen, favoring annealing to recover the surface quality of the sample.** However, the disadvantages of sample #4 might be considered if the sample cannot be annealed for $ex-situ$ characterization such as scanning electron microscopy (SEM), transmission electron microscopy (TEM) or Raman spectroscopy. In this context, preparation of samples without protective Te layers like sample #3 within preserving in dry $N_2$ box is preferable and more convenient for further measurement and fabrication.

## IV. CONCLUSIONS

In conclusion, we obtained nice stoichiometric films of mono-/double-layer $2H$-$MoTe_2$ by using a multi-step process and appropriate MBE conditions. The effect of exposing samples to air and $N_2$ atmosphere is carefully examined. It is clear that effects of oxidation impact significantly on the crystalline quality of the films, leading to certain difficulties in $ex-situ$ measurements. The full exposure of $MoTe_2$ films to air causes a complete change of the surface properties, making it no longer suitable for further characterization. In particular, it is impossible to recover clean $MoTe_2$ films. In this context, our work demonstrated an effective method to improve the efficiency of *ex-situ* sample transfer between vacuum chambers. **While capping with a protective layer is a well known practice, our experimental evidence by RHEED, STM and XPS shows that an inert atmosphere such as a dry nitrogen box, substantially preserves the crystalline quality of transfered films both capped with Te layers or not and makes it easier to recover the clean $MoTe_2$ surface**.

## V. ACKNOWLEDGMENTS

Trung T. Pham would like to thank ARES CCD for financial support. Roshan Castelino acknowledges a scholarship from the Jesuit province of l'EOF. We also would like to thank Etienne Gennart and Jean-Pierre Van Roy for technical support.



[1] P.K. Das, D. Di Sante, F. Cilento, C. Bigi, D. Kopic, D. Soranzio, A. Sterzi, J.A. Krieger, I. Vobornik, J. Fujii, and T. Okuda, Electronic properties of candidate type-II Weyl semimetal $WTe_2$: A review perspective, Electronic Structure 1, 1, 014003 (2019).
[2] C.C. Homes, M.N. Ali and R.J. Cava, Optical properties of the perfectly compensated semimetal $WTe_2$, Physical Review B 92, 16, 161109 (2015)
[3] C. Anichini, W. Czepa, D. Pakulski, A, Aliprandi, A. Ciesielski and P. Samori, Chemical sensing with 2D materials, Chemical Society Reviews 47, 13, 4860-4908 (2018).
[4] A.P. Gertych, A. Lapinska, K. Czerniak-Losiewicz, A, Duzynska, M. Zdrojek and J. Judek, Thermal properties of thin films made from $MoS_2$ nanoflakes and probed via statistical optothermal Raman method, Scientific reports 9, 13338 (2019).
[5] W. Choi, N. Choudhary, G.H. Han, J. Park, D. Akinwande and Y.H. Lee, Recent development of two-dimensional transition metal dichalcogenides and their applications, Materials Today 20, 3, 116-130 (2017).
[6] X. Ding, F. Peng, J. Zhou, W. Gong, G. Slaven, K.P Loh, C.T. Lim and D.T. Leong, Defect engineered bioactive transition metals dichalcogenides quantum dots, Nature communications 10, 41 (2019).
[7] I. G. Lezama, A. Arora, A. Ubaldini, C. Barreteau, E. Giannini, M. Potemski, and A.F. Morpurgo, Indirect-to-direct band gap crossover in few-layer $MoTe_2$, Nano letters 15, 4, 2336-2342 (2015).
[8] J. C. Park, S. J. Yun, H. Kim, J. H. Park, S. H. Chae, S. J. An, J. G. Kim, S. M. Kim, K. K. Kim, and Y. H. Lee, Phase-engineered synthesis of centimeter-scale 1T´ and 2H-molybdenum ditelluride thin films, ACS Nano 9, 6, 6548-6554, (2015).
[9] Trung T. Pham, Roshan Castelino, Alexandre Felten, and Robert Sporken, Preparation of single phase 2H-$MoTe_2$ films by molecular beam epitaxy, Applied Surface Science 523, 1, 146428 (2020).
[10] J. Gao and B. Li and J. Tan and P. Chow and T-M. Lu and N. Koratkar, Aging of transition metal dichalcogenide monolayers, ACS nano 10, 2, 2628-2635 (2016).
[11] J-H. Park, S. Vishwanath, X. Liu, H. Zhou, Sarah M. Eichfeld, Susan K. Fullerton-Shirey, Joshua A. Robinson, Randall M. Feenstra, J. Furdyna, D. Jena, H-G Xing, Andrew C. Kummel, Scanning tunneling microscopy and spectroscopy of air exposure effects on molecular beam epitaxy grown $WSe_2$ monolayers and bilayers, ACS nano 10, 4, 4258-4267 (2016).
[12] R. Addou, Christopher M Smyth, J-Y Noh, Y-C Lin, Y. Pan, S.M. Eichfeld, S. Folsch, J. A. Robinson, K. Cho, R. M. Feenstra, and R.M. Wallace, One dimensional metallic edges in atomically thin $WSe_2$ induced by air exposure, 2D Materials 5, 2, 025017 (2018).
[13] R. Duffy, P. Foley, B. Filippone, G. Mirabelli, D. O'Connell, B. Sheehan, P. Carolan, M. Schmidt, K. Cherkaoui, R. Gatensby, T. Hallam, G. Duesberg, F. Crupi, R. Nagle, and P. K. Hurley, Structural and electrical investigation of $MoS_2$ thin films formed by thermal assisted conversion of Mo metal, ECS Journal of Solid State Science and Technology 5, 11, Q3016-Q3020 (2016).
[14] R. Addou, S. McDonnell, D. Barrera, Z. Guo, A. Azcatl, J. Wang, H. Zhu, C. L. Hinkle, M. Quevedo-Lopez, H. N. Alshareef, L. Colombo, J. W. P. Hsu, and R. M. Wallace, Impurities and electronic property variations of natural $MoS_2$ crystal surfaces, ACS Nano 9, 9, 9124-9133 (2015).

[15] G. Mirabelli, C. McGeough, M. Schmidt, Eoin K. McCarthy, S. Monaghan, Ian M. Povey, M. McCarthy, F. Gity, R. Nagle, G. Hughes, A. Cafolla, Paul K. Hurley, R. Duffy, Air sensitivity of $MoS_2$, $MoSe_2$, $MoTe_2$, $HfS_2$, and $HfSe_2$, Journal of Applied Physics 120, 125102 (2016).
[16] X. Zheng, Y. Wei, C. Deng, H. Huang, Y. Yu, G. Wang, G. Peng, Z. Zhu, Y. Zhang, T. Jiang, S. Qin, R. Zhang and X. Zhang, Controlled layer-by-layer oxidation of $MoTe_2$ via $O_3$ exposure, ACS applied materials & interfaces 10, 36, 30045-30050 (2018).
[17] M. J. Mleczko, Andrew C. Yu, Christopher M. Smyth, V. Chen, Y-C Shin, S. Chatterjee, Y-C Tsai, Y. Nishi, Robert M. Wallace, and Eric Pop, Contact Engineering High-Performance n-Type $MoTe_2$ Transistors, Nano letters 19, 9, 6352-6362 (2019).
[18] H. Liu, N. Han, and J. Zhao, Atomistic insight into the oxidation of monolayer transition metal dichalcogenides: from structures to electronic properties, RSC Adv. 5, 23, 17572-17581 (2015).
[19] G. Firpo, F. Buatier de Mongeot, C. Boragno, and U. Valbusa, High performance portable vacuum suitcase, Review of scientific instruments 76, 026108 (2005).
[20] M. Lanius, Topological Insulating Tellurides: How to tune Doping, Topology, and Dimensionality, Doctoral dissertation, RWTH Aachen University (2018).
[21] S-K, Mo, C. Hwang, Y. Zhang, M. Fanciulli, S. Muff, J. Hugo Dil, Z-X Shen, and Z. Hussain, Spin-resolved photoemission study of epitaxially grown $MoSe_2$ and $WSe_2$ thin films, Journal of physics: Condensed matter 28, 45, 454001 (2016).
[22] P. M. Coelho, H. P. Komsa, K. Lasek, V. Kalappattil, J. Karthikeyan, M. H. Phan, Arkady V. Krasheninnikov, and M. Batzill, Room Temperature Ferromagnetism in $MoTe_2$ by Post Growth Incorporation of Vanadium Impurities, Advanced Electronic Materials 5, 5, 1900044 (2019).
[23] S. Tang, C. Zhang, D. Wong, Z. Pedramrazi, H-Z Tsai, C. Jia, B. Moritz et al., Quantum spin Hall state in monolayer 1T'-$WTe_2$, Nature Physics 13, 683-687 (2017).
[24] F. Ye, J. Lee, J. Hu, Z. Mao, J. Wei, and P. X. L. Feng, Environmental instability and degradation of singleand few-layer $WTe_2$ nanosheets in ambient conditions, Small 12, 42, 5802-5808 (2016).
[25] B. Chen, H. Sahin, A. Suslu, L. Ding, M. I. Bertoni, F. M. Peeters, and S. Tongay, Environmental changes in $MoTe_2$ excitonic dynamics by defects-activated molecular interaction, ACS Nano 9, 5, 5326-5332 (2015).
[26] H. Zhu, Q. Wang, L. Cheng, R. Addou, J. Kim, M. J. Kim, and R. M. Wallace, Defects and surface structural stability of $MoTe_2$ under vacuum annealing, ACS Nano 11, 11, 11005-11014 (2017).
[27] J. M. Woods, J. Shen, P. Kumaravadivel, Y. Pang, Y. Xie, G. A. Pan, M. Li, E. I. Altman, L. Lu, and J. J. Cha, Suppression of magnetoresistance in thin $WTe_2$ flakes by surface oxidation, ACS Appl. Mater. Interfaces 9, 27, 23175-23180 (2017).
[28] B. Sirota, N. Glavin, S. Krylyuk, A.V. Davydov, A.A. Voevodin, Hexagonal $MoTe_2$ with amorphous BN passivation layer for improved oxidation resistance and endurance of 2D field effect transistors, Scientific reports 8, 8668 (2018).
[29] J. C. Bernede, C. Amory, L. Assmann, and M. Spiesser, X-ray photoelectron spectroscopy study of $MoTe_2$ single crystals and thin films, Applied surface science 219, 3-4, 238-248 (2003).
[30] H.C. Diaz, R. Chaghi, Y. Ma, and M. Batzill, Molecular beam epitaxy of the van der Waals heterostructure $MoTe_2$ on $MoS_2$: phase, thermal, and chemical stability, 2D Materials 2, 4, 044010 (2015).
[31] X. Liu, D. Qu, Y. Yuan, J. Sun, and W. J. Yoo, Self-Terminated Surface Monolayer Oxidation Induced Robust Degenerate Doping in $MoTe_2$ for Low Contact Resistance, ACS Appl. Mater. Interfaces 12, 23, 26586-26592 (2020).
[32] L. Yang, H. Wu, W. Zhang, Z. Chen, J. Li, X. Lou, Z. Xie, R. Zhu, and H. Chang, Anomalous oxidation and its effect on electrical transport originating from surface chemical instability in large-area, few-layer 1T'-$MoTe_2$ films, Nanoscale 10, 42, 19906-19915 (2018). Q. Liu, H. Qin, J.A. Boscoboinik and G. Zhou, Comparative study of the oxidation of NiAl (100) by molecular oxygen and water vapor using ambient-pressure X-ray photoelectron spectroscopy, Langmuir 32, 44, 11414-11421 (2016).
[33] C. H. Naylor, W. M. Parkin, J. Ping, Z. Gao, Y. R. Zhou, Y. Kim, F. Streller, R. W. Carpick, A. M. Rappe, M. Drndicc, J. M. Kikkawa, and A. T. Charlie Johnson, Monolayer Single-Crystal 1T'- $MoTe_2$ Grown by Chemical Vapor Deposition Exhibits Weak Antilocalization Effect, Nano Lett. 16, 7, 4297-4304 (2016).